Applied Catalysis B: Environmental 121–122 (2012) 162–170

Contents lists available at SciVerse ScienceDirect

Applied Catalysis B: Environmental

journal homepage: www.elsevier.com/locate/apcatb

# Activity, selectivity and stability of praseodymium-doped $CeO_2$ for chlorinated VOCs catalytic combustion

B. de Rivas[a], N. Guillén-Hurtado[b], R. López-Fonseca[a], F. Coloma-Pascual[b], A. García-García[b], J.I. Gutiérrez-Ortiz[a], A. Bueno-López[b,*]

[a] Department of Chemical Engineering, Faculty of Science and Technology, University of the Basque Country, PO Box 644, E-48080 Bilbao, Spain
[b] Department of Inorganic Chemistry, University of Alicante, Campus Sant Vicent s/n, PO Box 99, E-03080 Alicante, Spain

ARTICLE INFO

*Article history:*
Received 28 January 2012
Received in revised form 24 March 2012
Accepted 27 March 2012
Available online 4 April 2012

*Keywords:*
Chlorinated VOC combustion
1,2-Dichloroethane
$Ce_xPr_{1-x}O_2$
Cerium–praseodymium mixed oxide

ABSTRACT

Ce–Pr mixed oxides, namely $Ce_{0.8}Pr_{0.2}O_2$, $Ce_{0.5}Pr_{0.5}O_2$ and $Ce_{0.2}Pr_{0.8}O_2$, were prepared by conventional coprecipitation and evaluated for the catalytic combustion of 1,2-dichloroethane, which was selected as a model reaction for chlorinated VOC abatement. For comparison purposes, the pure oxides were also prepared and catalytically tested. A certain decrease in catalytic activity was observed after three consecutive temperatures cycles from 150 to 500 °C for all catalysts, except for $Ce_{0.5}Pr_{0.5}O_2$. This deactivation was particularly noticeable for pure praseodymia and $Ce_{0.2}Pr_{0.8}O_2$, while $Ce_{0.8}Pr_{0.2}O_2$ and $Ce_{0.5}Pr_{0.5}O_2$ exhibited a superior stability. The catalysts deactivation was attributed to bulk and/or surface chlorination, as revealed by X-ray diffraction, Raman spectroscopy and X-ray photoelectron spectroscopy. Interestingly, the $Ce_{0.5}Pr_{0.5}O_2$ mixed oxide, which converted the chlorinated feed at the lowest temperature due to its substantial resistance to chlorination, showed a constant activity in a 115 h lifetime test at 335 °C.



## 1. Introduction

The release of volatile organic compounds (VOCs) to the atmosphere results in tangible environmental damage. These pollutants can contribute to atmospheric processes which can have detrimental effects on human health. For example, VOCs have been implicated in the formation of ground level ozone, ozone depletion and they often act as greenhouse gases. In September 2005, the Commission of the European Communities in the Framework of the "Clean Air for Europe" (CAFE) Programme published its Thematic Strategy on Air Pollution [1]. This strategy sets health and environmental objectives and emission reduction targets for the main pollutants. More specifically, its aim is to cut the annual number of premature deaths caused by air pollution by 40% in 2020, with regard to the 2000 level, and to reduce the continuing damage of the Europe's ecosystems. To achieve these objectives, emissions of sulphur dioxide must be reduced by 82%, nitrogen oxides by 60%, volatile organic compounds by 51%, ammonia by 27% and fine particulate matter by 59%.

A number of VOCs with different chemical composition are emitted by different sources (off-gases from chemical plants, groundwater decontamination by air stripping, odour emission control, and contaminated air in solvent evaporation processes). Chlorohydrocarbons are among the most difficult to abate by catalytic combustion. Chlorinated compounds require special attention due to their toxicity, high stability and widespread application in industry [2]. Consequently, to develop efficient catalysts for low-temperature complete destruction of chlorinated VOCs is a challenging task of ongoing interest [3]. As an alternative to noble metals and transition metal oxides, cerium-based oxides are promising catalysts [4–6]. Ceria-based materials are able to undergo a rapid and reversible $Ce^{4+}/Ce^{3+}$ redox cycles at moderate temperatures due to the high oxide-ion mobility in the solid state from surface to bulk and vice versa. In many cases, the redox properties and chemical activity of pure ceria could be enhanced by introducing dopant cations into the oxide lattice. In this sense, considerable attention has been paid to incorporate variable valence ions into the ceria lattice to recognise their role on defect chemistry. The oxygen atoms/vacancies attached to reducible elements are mobile, which could contribute to the oxygen storage/release capability of mixed oxides [7]. Among the reducible elements, praseodymium is particularly suitable to obtain solid solutions with ceria. The structure of $Pr_6O_{11}$ is fluorite type, and the ionic radius of $Pr^{4+}$ (0.096 nm) is close to that of $Ce^{4+}$ (0.097 nm). In the mixed oxide, it can form mixed oxidation states with both $Pr^{3+}$ and $Pr^{4+}$ cations. Further, in ceria–praseodymia solid solutions, both elements can adopt 3+ and 4+ oxidation states, and the anion vacancies are much mobile in this system [8]. In summary, the insertion of praseodymium within the fluorite host lattice of $CeO_2$ provides new

* Corresponding author at: Inorganic Chemistry Department, University of Alicante, Ap. 99, E03080, Alicante, Spain. Tel.: +34 600948665; fax: +34 965903454.
*E-mail address:* agus@ua.es (A. Bueno-López).

0926-3373/$ – see front matter © 2012 Elsevier B.V. All rights reserved.
http://dx.doi.org/10.1016/j.apcatb.2012.03.029

**Table 1**
Ce/Pr ratio on fresh Ce–Pr mixed oxides determined by TEM-EDS and XRF.

| | Ce/Pr nominal atomic ratio | EDS-determined Ce/Pr atomic ratio | XRF-determined Ce/Pr atomic ratio |
|---|---|---|---|
| Ce80Pr20 | 4 | 3.69 | 3.64 |
| Ce50Pr50 | 1 | 0.87 | 0.85 |
| Ce20Pr80 | 0.25 | 0.22 | 0.19 |

materials with interesting catalytic properties for environmental applications, such as automotive three-way catalysts [9,10], $NO_x$-trap catalysts [11], $N_2O$ decomposition [12], CO oxidation [13,14], light hydrocarbons (methanol and methane) combustion [13,15] and soot removal [16,17]. However, to the best of our knowledge, there are no reports on the viability of Ce–Pr mixed oxides for the gas-phase oxidative combustion of chlorinated compounds.

In this paper, the catalytic activity, selectivity and stability of a series of Ce–Pr mixed oxides with different composition were investigated in a fixed-bed flow reactor. The synthesised mixes oxides were characterised using X-ray diffraction (XRD), $N_2$-physisorption at low temperature, X-ray photoelectron spectroscopy (XPS), Raman spectroscopy (RS), and temperature programmed reduction by $H_2$ ($H_2$-TPR). 1,2-Dichloroethane (DCE; or ethylene dichloride or $C_2H_4Cl_2$) was chosen as model short-chain chlorinated VOC. This compound is probably one of the most important chlorinated VOC emitted in gaseous industrial waste streams since it is used as an intermediate for the production of polyvinyl chloride, and as a solvent in textile cleaning and metal degreasing [18,19].

## 2. Experimental

### 2.1. Samples preparation

Ceria–praseodymia ($Ce_xPr_{1-x}O_2$, $x$ = 0.2, 0.5 and 0.8) mixed oxides were prepared by a coprecipitation method, using $Ce(NO_3)_3{\cdot}6H_2O$ (supplied by Aldrich, 99.99%) and $Pr(NO_3)_3{\cdot}6H_2O$ (supplied by Sigma Aldrich, 99.9%) as precursors. The samples are referred to as Ce20Pr80, Ce50Pr50 and Ce80Pr20, respectively. The required amounts of each precursor were dissolved in water under mild stirring conditions. Upon complete dissolution, ammonium hydroxide was added drop wise until the precipitation was complete (pH ~9). The accumulated mixed oxide/hydroxide paste was recovered by filtration. It was then dried in an oven at 110 °C for 24 h, and subsequently calcined at 500 °C for 1 h in static air. Both pure cerium oxide (Ce100) and praseodymium oxide (Pr100) were also prepared for comparison purposes by adopting the same precipitation method. The actual Ce/Pr ratios of the Ce–Pr mixed oxides were determined by TEM-EDS and XRF and are compiled in Table 1. All mixed oxides show values slightly lower than the corresponding nominal Ce/Pr ratio. This could be attributed to the fact that $Ce(OH)_3$ is slightly more soluble than $Pr(OH)_3$ ($K_{sp} = 1.5 \times 10^{-20}$ and $3.39 \times 10^{-24}$, respectively).

In order to perform the catalytic tests, catalyst pellets with diameter from 0.3 to 0.5 mm were prepared by compressing the oxide powders flakes in a hydraulic press (Specac), followed by crushing and sieving.

### 2.2. Catalytic tests

The oxidation of 1,2-dichloroethane was chosen as a measure to assess the performance of the prepared Ce-Pr catalysts. 1,2-Dichloroethane was taken as a model compound for the category of double carbon chlorinated VOC with a H/Cl ratio of >1. This compound is typically ranked as intermediate-high on its ease of destruction when compared, for instance, with double carbon olefins such as dichloroethylene and trichloroethylene [20,21]. The activity of the bulk catalysts was examined by analysing three consecutive combustion tests between 150 and 500 °C. The combustion experiments consisted of increasing the temperature in steps of 25 °C between 150 and 500 °C, and the catalyst was then cooled to 150 °C. This cycle was repeated three times using the same catalyst sample. $T_{50}$ parameter (temperature needed to attain 50% conversion) was used as criterion for evaluating the catalytic performance. Catalytic tests were carried out in a bench-scale fixed bed reactor (microactivity modular laboratory system provided by PID Eng&Tech S.L.) operated at atmospheric pressure and fully monitored by computer. The reactor was made of quartz with an internal diameter of 10 mm and a height of 300 mm, in which the temperature is controlled by a thermocouple placed in the catalyst bed. Typically, 0.85 g of catalyst pellets (0.3–0.5 mm) was loaded. The reaction feed consisted of 1000 ppm of DCE in dry air with a total gas flow of 500 $cm^3\ min^{-1}$. The amount and granulometric fraction of catalyst and the total gaseous stream were chosen in order to be in true kinetic regime, namely, to be out of the internal and external diffusion limits, and to reach a gas hourly space velocity of 30,000 $h^{-1}$, which corresponds to the conditions usually met in the exhaust gases from industrial units. Conversion data were calculated by the difference between inlet and outlet concentrations. Conversion measurements and product profiles were taken at steady state, typically after 30 min on stream. The product selectivity was calculated based on either chlorine or carbon atoms present in that product divided by the total chlorine or carbon atoms, respectively, present in the product stream (expressed as %), according to the following equations ($C_xH_yCl_z$ corresponds to the chlorinated by-products that may result from the incomplete combustion of the feed molecule).

$$S_{HCl} = \frac{[HCl]}{[HCl] + 2[Cl_2] + z\left[C_xH_yCl_z\right]} \times 100 \quad (1)$$

$$S_{Cl_2} = \frac{2[Cl_2]}{[HCl] + 2[Cl_2] + z\left[C_xH_yCl_z\right]} \times 100 \quad (2)$$

$$S_{CO_2} = \frac{[CO_2]}{[CO] + [CO_2] + x\left[C_xH_yCl_z\right]} \times 100 \quad (3)$$

The feed and effluent streams were analysed using an on-line 7980A Agilent Technologies gas chromatograph equipped with a thermal conductivity detector (for CO and $CO_2$) and an electron capture detector (for chlorinated hydrocarbons). Analysis of HCl and $Cl_2$ was carried out by means of ion selective electrode and titration, respectively. The experimental error of the GC analysis was <1% while the experimental error for the quantification of HCl and $Cl_2$ was <3%. Further details on analytical procedures were described elsewhere [22].

### 2.3. Samples characterisation

The BET surface areas of the samples were determined by multi-point $N_2$ adsorption at −196 °C using an automatic Autosorb-6B (Quantachrome equipment). The samples were previously degassed for 4 h at 250 °C under vacuum.

Powder XRD patterns were recorded in a Bruker D8 advance diffractometer, using CuKα radiation. Diffractograms were registered between 10 and 60° (2$\theta$) with a step of 0.02° and a time per step of 3 s.

Raman spectra were obtained in a Bruker RFS 100/S Fourier transform raman spectrometer with a variable power Nd:YAG laser source (1064 nm). The power was fixed at 100 mW and 512 scans were done to obtain each spectrum.

The actual composition of the Ce–Pr mixed oxides was determined with a TEM microscope-coupled EDS analyser (OXFORD,

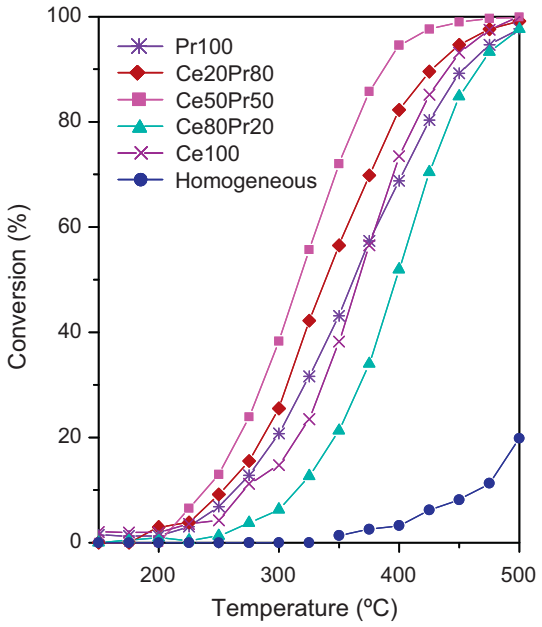


**Fig. 1.** Light-off curves of DCE combustion during the third reaction cycle.

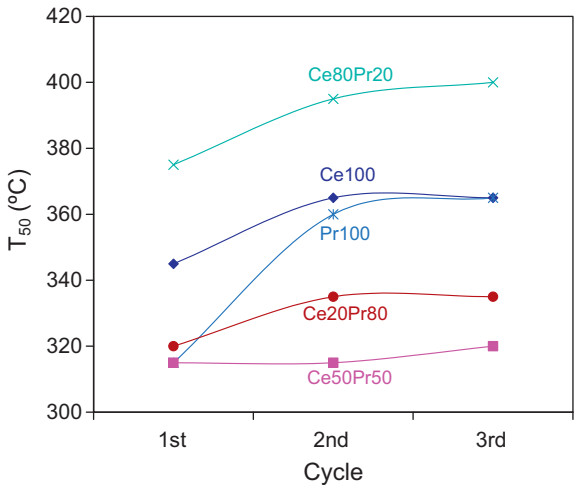


**Fig. 2.** $T_{50}$ temperature for three consecutive DCE catalytic combustion cycles.

model INCA Energy TEM100) by analysing spots of 500 nm diameter, and also by XRF in a PHILIPS MAGIX PRO device (model PW2400) equipped with a rhodium X-ray tube and beryllium window.

The reducibility of the catalysts was examined by $H_2$-temperature programmed reduction ($H_2$-TPR) in a Micromeritics Pulse ChemiSorb 2705 device consisting of a tubular quartz reactor coupled to a TCD detector. The reducing gas used was 5% $H_2$ in Ar, with a flow rate of 35 ml/min. The temperature range explored was from room temperature to 1000 °C at a heating rate of 10 °C/min. Before the reduction, the catalysts were pretreated in situ at 500 °C for 1 h with a gas flow of 5% $O_2$/He.

XPS characterisation of the catalysts was carried out in a VG-Microtech Multilab electron spectrometer using a MgKα (1253.6 eV) radiation source. To obtain the XPS spectra, the pressure of the analysis chamber was maintained at $5 \times 10^{-10}$ mbar. The binding energy (BE) and the kinetic energy (KE) scales were adjusted by setting the C 1s transition at 284.6 eV, and BE and KE values were determined with the Peak-fit software of the spectrometer. The $Ce^{3+}$ (%), with regard total cerium, was calculated with the procedure reported by Romeo et al. [23] and the $Pr^{3+}$(%), with regard to total praseodymium, was estimated as proposed by Borchet et al. [24].

## 3. Results and discussion

### 3.1. Catalytic tests

The non-catalytic reaction (the catalyst was replaced by inert quartz particles) was first investigated. DCE conversion in the absence of any catalyst did not start up to 350 °C, and reached only 20% conversion at 500 °C. In contrast, as it is observed in Fig. 1, which includes the light-off curves of the third reaction cycle for each investigated sample, the use of Ce–Pr mixed oxides as catalysts outstandingly accelerated the desired reaction, and in all cases the chlorinated compound was completely abated between 450 and 500 °C. During this third cycle, the most active catalyst among those tested was that with equimolar proportions of cerium and praseodymium (Ce50Pr50).

Fig. 2 shows the $T_{50}$ values corresponding to three consecutive reaction cycles performed with the examined catalysts. As a general trend, $T_{50}$ increased after consecutive cycles for most catalysts, and this consequently resulted in a decrease in the catalytic activity. The largest increase in $T_{50}$ was noticed between the first and second cycles, while $T_{50}$ remained relatively stable after the second cycle for most catalysts. These results evidenced a certain deactivation of most catalysts during the first cycle, which was attributed, as it will be discussed in detail afterwards, to the progressive chlorination of the oxides.

Interestingly, insertion of certain amounts of praseodymium into the ceria lattice involved a positive effect on the activity of the resulting mixed oxide. Particularly, the sample with equimolar Ce and Pr contents, Ce50Pr50, was the most active and stable catalyst. Another important observation was that fresh Pr100 oxide exhibited a notable activity, which was remarkably higher than that of fresh Ce100 and comparable with that of Ce50Pr50. However, the conversion dramatically decreased after the first temperature cycle, resulting in a high $T_{50}$ value of 360 °C. On the basis of the $T_{50}$ values in the third reaction cycle, where the catalytic performance could be considered invariable, the following trend could be noted:

$$Ce50Pr50 > Ce20Pr80 > Ce100 \sim Pr100 > Ce80Pr20$$

Accordingly, Luo et al. [13] and Krishna et al. [16] also found a superior catalytic activity in the oxidation of recalcitrant compounds, namely methane and model diesel soot, respectively, for the Ce–Pr mixed oxide with an equimolar composition. Moreover, in both cases the combustion temperatures were appreciably lowered with respect to those of the pure oxides.

High conversion at low temperatures is not the only criterion to identify good chlorinated VOC combustion catalysts. The desired reaction pathway is the conversion of chlorinated VOC to deep oxidation products, that is, $H_2O$, $CO_2$ and HCl or $Cl_2$. However, the combustion of chlorinated VOCs may also yield carbon monoxide and highly chlorinated by-products, which are sometimes even more toxic and recalcitrant than the starting material.

The product distribution was analysed and CO, $CO_2$, HCl and $Cl_2$ were the main products for all catalysed combustions (see Fig. 3). As a general behaviour, the conversion of chlorine atoms to HCl over the mixed oxide catalysts was favoured with respect to $Cl_2$ formation at temperatures lower than 375–400 °C. At higher temperatures, significant amounts of molecular chlorine were also formed due to the occurrence of the Deacon reaction ($2HCl + 1/2O_2 \leftrightarrow Cl_2 + H_2O$). As a result, selectivity to $Cl_2$ (Eq. (2)) was about 50–60% at 450–500 °C.

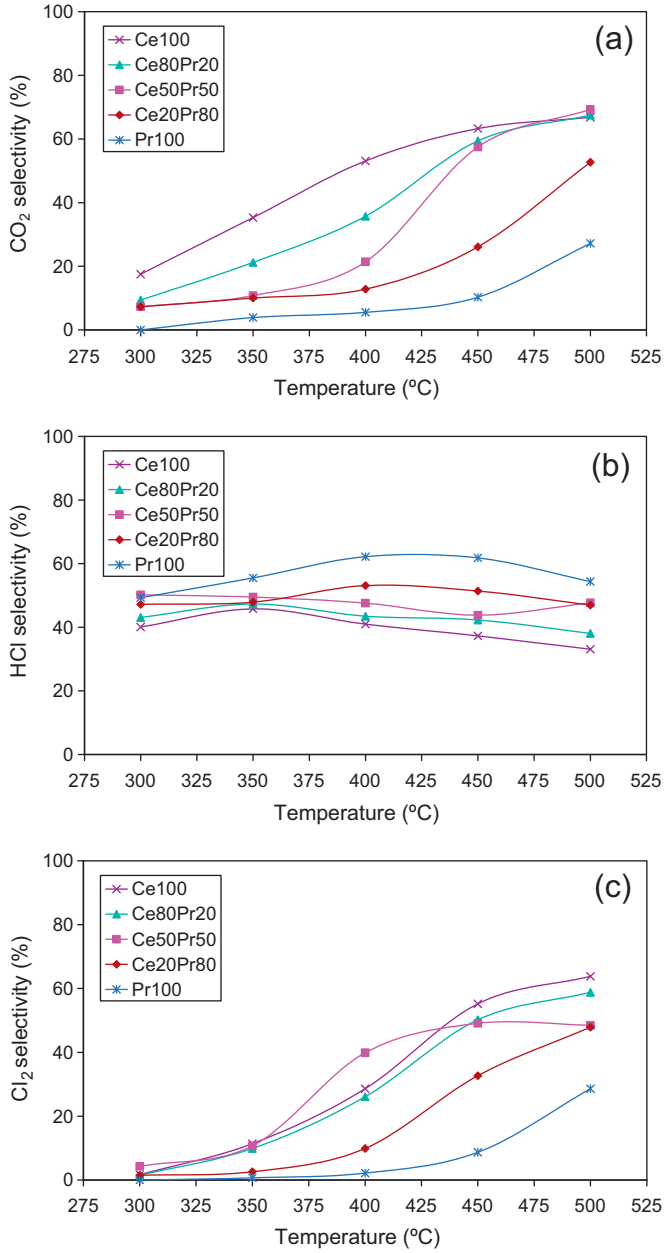


**Fig. 3.** Selectivity to main products during the third reaction cycle.

As it is observed in Fig. 4, the combustion also yielded in some cases vinyl chloride, as a consequence of the dehydrochlorination of the feed [25], and trace amounts (<8 ppm) of other chlorinated hydrocarbons, principally methyl chloride and carbon tetrachloride (profiles not shown for the sake of brevity).

Regarding the conversion to carbon oxides, the selectivity towards $CO_2$ gradually increased with temperature and ceria content in the mixed oxide (Fig. 3). As a result, at 450 °C, $CO_2$ selectivity (Eq. (1)) values of about 58% were found over Ce50Pr50 and Ce80Pr20, while it was slightly higher (63%) over the pure ceria sample (Ce100). The notable performance of $CeO_2$ for CO oxidation has been previously reported in the oxidation of hydrocarbons [4].

Finally, a lifetime test was performed with the most active mixed oxide (Ce50Pr50) at constant temperature (335 °C), which was conducted for 115 h. As it is observed in Fig. 5, the conversion remained stable for such a long period of time. The products distribution during this lifetime test evidenced that the selectivity to products also remained unaffected, with a vinyl chloride concentration of about

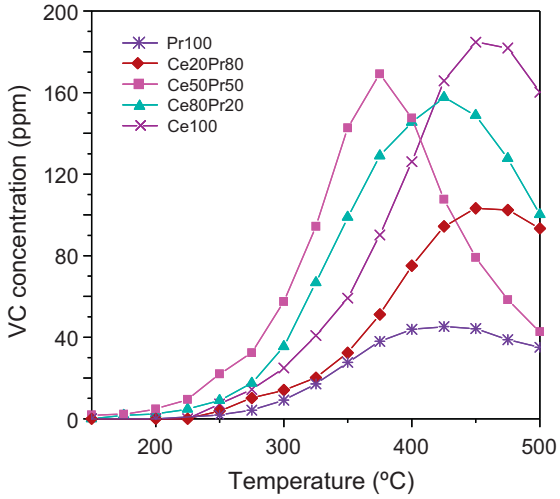


**Fig. 4.** Evolution of vinyl chloride (VC) with temperature during the third reaction cycle.

100 ppm and a selectivity towards deep oxidation products of 25% (Eq. (3)) for $CO_2$ (220 ppm) and 50% (Eq. (1)) for HCl (250 ppm HCl).

### 3.2. $H_2$-TPR characterisation of fresh catalysts

$H_2$-TPR characterisation included in Fig. 6 provides some information about the catalytic performance of the fresh oxides. The catalyst Ce100 shows the typical $H_2$ reduction profile of this material, with two well-defined peaks attributed to surface and bulk reduction at 400–600 °C and 800–1000 °C, respectively.

The bulk reduction band disappeared for Pr-containing catalysts, evidencing improved reducibility with regard to pure ceria, and the higher the Pr content, the higher the area under the reduction peak. The percentage of $Ln^{4+}$ ($Ce^{4+} + Pr^{+4}$) reduced to $Ln^{3+}$ in each catalyst was calculated and data are compiled in Table 2. An increase in the reduction percentage was found from 10.9% for the surface reduction of pure ceria to 60.2% for pure praseodymia reduction.

In Pr-containing catalysts, the reduction band showed more than a single contribution, with shoulders or two well defined maxima. This could be attributed to the different reducibility of $Ce^{4+}$ and $Pr^{4+}$ cations in mixed oxides, and would be an evidence of the presence of segregated phases, as it will be discussed in detail in the coming sections. The release or reduction of some surface

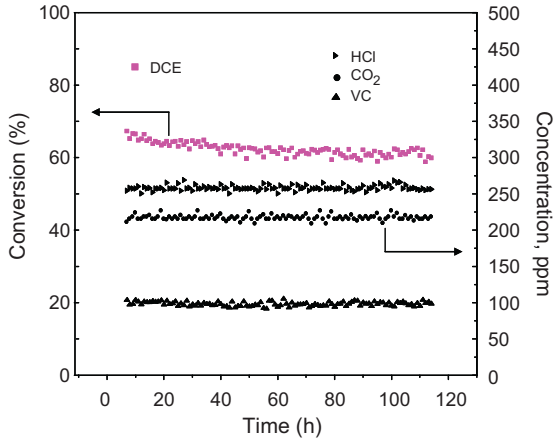


**Fig. 5.** Lifetime test performed with Ce50Pr50 at 335 °C (DCE stands for 1,2-dichloroethane; VC stands for vinyl chloride).

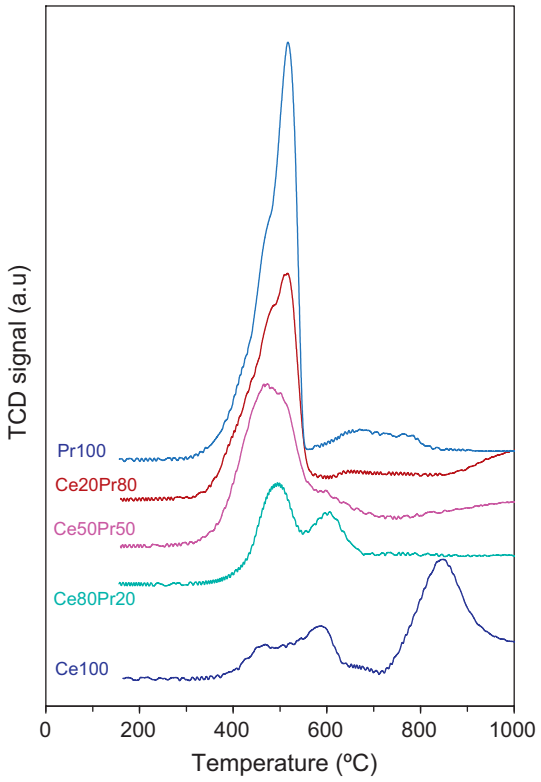


**Fig. 6.** $H_2$-TPR characterisation of fresh catalysts.

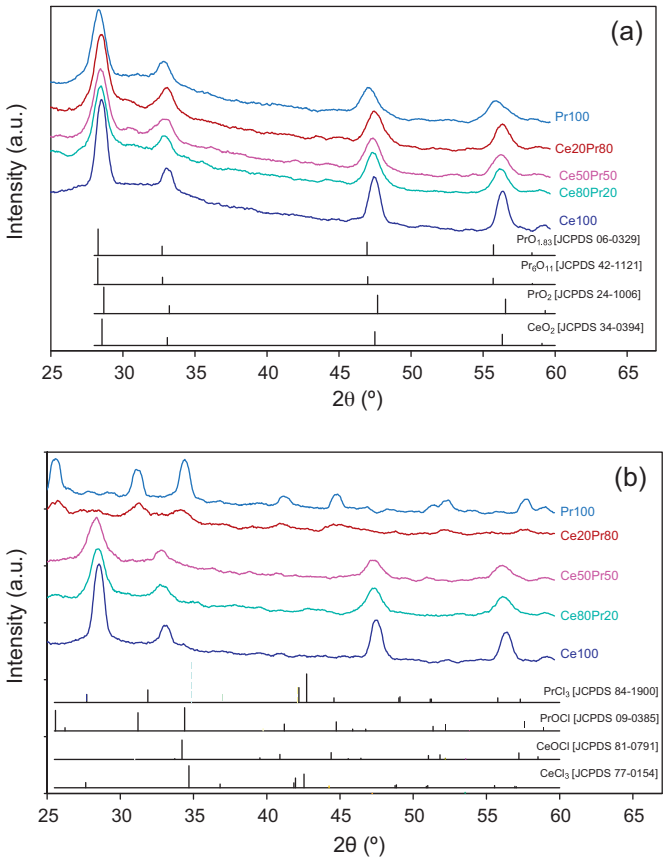


**Fig. 7.** X-Ray diffractograms of fresh (a) and used catalysts (after three DCE oxidation cycles between 150 and 500 °C) (b) and representative reference patterns.

species, like carbonates or hydroxyls, among other surface species, could also contribute to the $H_2$-TPR profiles at temperatures around 500 °C.

The lowest $H_2$ reduction onset temperature (around 335 °C) and the largest $H_2$ consumption areas were found for the Pr100, Ce20Pr80 and Ce50Pr50 samples (Fig. 6). Note that these three catalysts showed the highest catalytic activity during the first reaction cycle (see Fig. 2). Among them, the most symmetric $H_2$-TPR band (this symmetry could be taken as an indirect evidence of structural homogeneity) corresponded to Ce50Pr50, this being the most stable catalyst. On the contrary, Ce100 and Ce80Pr20 catalysts, with a lower catalytic activity during the first cycle than the Pr-rich and equimolar formulations (see Fig. 2), presented two clear maxima on the surface reduction band. It is also noteworthy that the onset temperature of this band was also higher (around 400 °C).

These $H_2$-TPR results suggested that the Ce-Pr catalyst followed a redox DCE combustion mechanism, which is usual for ceria-based catalysts, and the improved reducibility induced by large amounts of Pr had a positive effect on the catalytic activity of the fresh catalysts. This redox cycle, which can be accomplished either by Ce and Pr oxides, is expected to be hindered by oxychlorides formation, thus explaining the observed inhibition of some catalysts upon chlorination. In addition, surface chlorination is expected to block gas adsorption sites, also contributing to catalysts inhibition. These arguments are analysed in detail in the coming sections.

**Table 2**
Percentage of $Ln^{4+}$ reduced to $Ln^{3+}$ with regard to total Ln content in $H_2$-TPR experiments (Ln = Ce + Pr).

| | $Ln^{4+}$ reduced (%) |
|---|---|
| Ce100 | 10.9 (LTP) and 17.0 (HTP) |
| Ce80Pr20 | 23.4 |
| Ce50Pr50 | 43.5 |
| Ce20Pr80 | 40.9 |
| Pr100 | 60.2 (LTP) and 4.2 (HTP) |

LTP = low-temperature peak; HTP = high-temperature peak.

### 3.3. Structural and surface characterisation of fresh and used catalysts

#### 3.3.1. Structural characterisation by XRD, $N_2$ adsorption and Raman spectroscopy

Fig. 7 shows the X-ray diffractograms of fresh (Fig. 7a) and used catalysts (Fig. 7b; after three DCE oxidation cycles between 150 and 500 °C) together with representative reference patterns. As expected, the fresh ceria sample Ce100 presented the typical fluorite structure of this material ([JCPDS file: 34-0394]).

The diffractograms of Pr-containing samples are more complicated to be interpreted, because Pr can form several stoichiometric and non-stoichiometric sub-oxides with formula $PrO_x$ where $x \leq 2$, which would present diffraction patterns only slightly different to that of fluorite ceria. The XRD peaks of fresh praseodymia (Pr100 sample) were asymmetric, suggesting the presence of more than one praseodymium oxide. The shift of the peaks toward lower angles with regard to the position of pure ceria peaks was consistent with the formation of $PrO_{1.83}$ or $Pr_6O_{11}$ [JCPDS file: 06-0329 and 42-1121, respectively] and the shoulders at high angles suggested the presence of $PrO_2$ as well [JCPDS file: 24-1006].

The XRD peaks of the fresh Ce80Pr20, Ce50Pr50 and Ce20Pr80 mixed oxides appeared at the same positions than those of pure ceria (Ce100), and the formation of a main fluorite phase could be inferred. However, the mixed oxide peaks were asymmetric, with shoulders at both sides of the main peak that suggested the presence of segregated phases of praseodymium oxide of different stoichiometry.

**Table 3**
BET surface area ($m^2/g$) of the fresh and used catalysts (after three DCE oxidation cycles between 150 and 500 °C).

| | Fresh | Used |
|---|---|---|
| Ce100 | 47 | 40 |
| Ce80Pr20 | 53 | 42 |
| Ce50Pr50 | 30 | 52 |
| Ce20Pr80 | 28 | 64 |
| Pr100 | 43 | 33 |

The X-ray diffractograms of the used samples (Fig. 7b) evidenced the accumulation of chlorine on some catalysts during the DCE combustion tests, which explained the partial deactivation deduced from Fig. 2. The fluorite structure was observed in the diffractograms of cerium-rich and equimolar samples Ce100, Ce80Pr20 and Ce50Pr50, while not in those of praseodymium-rich catalysts (Ce20Pr80 and Pr100). The diffractograms of Ce20Pr80 and Pr100 revealed the formation of PrOCl [JCPDS file: 09-0385], being much more crystalline the phase formed on Pr100 than that on Ce20Pr80, with narrower and more intense XRD peaks. PrOCl is quite stable and can only be oxidatively dechlorinated at temperatures exceeding 1000 °C, as demonstrated by Yang et al. [26].

The catalyst Ce50Pr50, which was the most active and stable one (see Figs 1 and 2), did not present any evidence of chlorination. The most important change in the diffractogram of this sample after the catalytic tests was a broadening of the XRD peaks and a decrease in intensity, with regard to the fresh sample, which could be related to a decrease in the crystallite size during the course of the reactions. This decrease in crystallite size was consistent with the increase in BET surface area from 30 to 52 $m^2/g$ before and after the catalytic tests, respectively (see Table 3). The changes in BET areas of the remaining samples during the catalytic tests could be also related to the structural changes as deduced from XRD.

Raman spectroscopy characterisation confirmed most conclusions of the XRD characterisation. Raman spectra of fresh and used catalysts, after three DCE oxidation cycles between 150 and 500 °C, are compiled in Fig. 8a and b, respectively. The Raman spectra of fresh ceria Ce100 presented the $F_{2g}$ band at 464 $cm^{-1}$ characteristic of this material while pure praseodymia Pr100 showed an almost flat spectrum under the conditions used for the measurements. The Ce–Pr mixed oxides also presented the $F_{2g}$ fluorite peak, but the intensity was much lower than that of pure ceria. One of the reasons of this decrease could be the introduction of Pr cations into the fluorite structure of ceria, which would deform the lattice affecting the oxygen breathing, and at the end, the $F_{2g}$ signal intensity. However, in Pr-containing samples, the Raman signals intensity must be interpreted very carefully because the fluorescence produced by Pr affects intensity. Much more concluding was the position of the $F_{2g}$ peak, which shifted towards low Raman shifts with the Pr content of the mixed oxide. This shift could be attributed to the introduction of $Pr^{3+}$ cations (larger than $Ce^{4+}$) into the ceria framework. As it is observed in Fig. 9, a linear relationship between Pr loading and peak position was obtained. On one hand, this was an evidence of the introduction of Pr cations within the fluorite lattice of ceria, and on the other hand, this relationship confirmed that the amount of Pr inserted into the fluorite lattice was proportional to the nominal percentage of Pr on the mixed oxides. The ceria fluorite framework was confirmed by the presence of a narrow peak at around 100 $cm^{-1}$, as reported by Luo et al. [13].

In agreement with XRD analysis, the Raman spectra of the cerium-rich and equimolar samples (Ce100, Ce80Pr20 and Ce50Pr50) after the catalytic tests (Fig. 8b) were quite similar to the counterpart spectra of the fresh samples (Fig. 8a), with typical features of pure ceria structure for used Ce100, and of Ce–Pr solid solutions for used Ce80Pr20 and Ce50Pr50. If $CeCl_3$ or CeOCl phases were formed, additional Raman bands would be expected

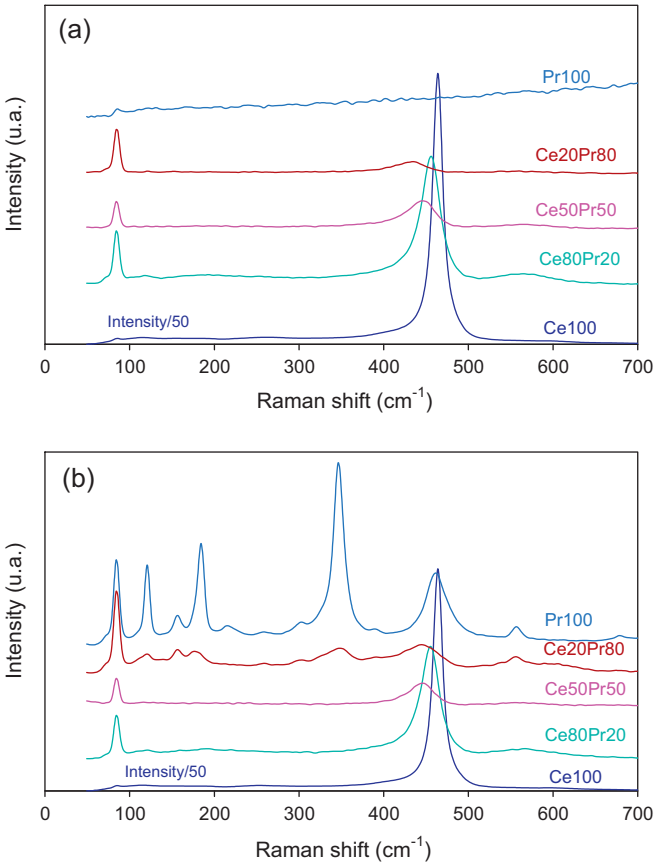


**Fig. 8.** Raman spectra of fresh (a) and used catalysts (after three DCE oxidation cycles between 150 and 500 °C) (b).

at 177 and 208 $cm^{-1}$ for $CeCl_3$ and at 119 and 327 $cm^{-1}$ for CeOCl [27], and this was not the case. On the contrary, and also in accordance with the formation of chlorinated species observed by XRD, the Raman spectra of used Pr100 and Ce20Pr80 clearly showed a change of the solid structure after the catalytic tests. The examination of the Raman spectra indicated the presence of new bands (not existing in the fresh samples), which could be attributed to PrOCl. It is known that a Matlockite-type (PbFCl) structure is stable for the lighter rare-earth oxychlorides (Re = La–Er) [28]. This structure is tetragonal, with a *P4/nmm* space group. Several vibrational modes (up to 15) are expected in a $D_{4h}$ symmetry group [29,30], thus explaining the bands now appearing for these two used

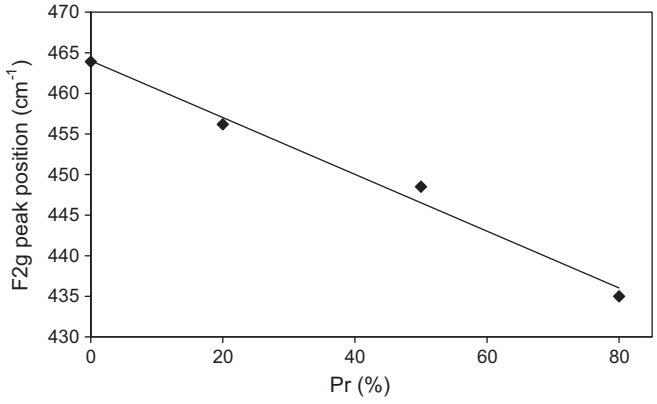


**Fig. 9.** $F_{2g}$ Raman peak position of cerium-containing fresh catalysts as a function of the Pr molar percentage (with regard to total Ce + Pr).

catalysts, instead of the single $F_{2g}$ mode of a fluorite-cubic structure. In particular, the Raman spectrum corresponding to Pr100 used was very similar to that found in the literature for LaOCl [29,30].

As a summary, this structural characterisation allows concluding that the $Ce_xPr_{1-x}O_2$ samples form mixed oxides with introduction of Pr cations onto the parent ceria lattice, but the presence of segregated phases of the pure oxides could not be ruled out. After the catalytic tests, the Pr-rich formulations (Pr100 and Ce20Pr80) underwent a more severe chlorination with PrOCl formation. The most active and stable catalyst (Ce50Pr50) did not show clear evidences of chlorination, and only minor structural changes were observed during the catalytic tests (only an increase in the BET surface area which was consistent with a decrease in the crystallite size).

### 3.3.2. Surface characterisation by XPS

In order to deepen into the catalysts deactivation processes, surface characterisation of the fresh and used catalysts was conducted by means of XPS. Table 4 lists some representative parameters obtained from this XPS analysis.

The Ce/Pr ratios for the fresh ceria–praseodymia samples were always lower than the nominal values, revealing Pr enrichment on the particles surface. For these estimations, the Ce 3d and Pr 3d levels were used, whose corresponding binding energies are not very different (870 and 970 eV, respectively). This corresponded to comparable kinetic energy and thus comparable analysis depth. This degree of praseodymium enrichment on the surface was similar to that found by other authors (for instance, a Ce/Pr ratio of 1.76 has been reported for a commercial $Ce_{0.81}Pr_{0.19}O_2$ mixed oxide [31]).

An increase in the Ce/Pr ratio was noted for the used Ce20Pr80 catalyst with regard to the fresh one, thereby suggesting important chemical modifications during the DCE combustion tests. On the contrary, the most stable catalyst Ce50Pr50 hardly showed any variation in its Ce/Pr ratio.

The $Cl_{2p}$ electronic transition was detected in all used catalysts, confirming the presence of chlorine surface species. The range of binding energies corresponding to these $Cl_{2p}$ transitions is depicted in Fig. 10. All used catalysts showed a peak at 198 eV that was assigned to chlorine on the species PrOCl and/or CeOCl. The intensity of this peak was much higher for Pr100 and Ce20Pr80 than for the remaining catalysts, which was in agreement with the considerably higher degree of chlorination observed by bulk techniques (Raman spectroscopy and XRD) for the Pr-rich catalysts. The Cl/(Ce + Pr) atomic ratios, compiled in Table 4, were around 1 for Pr100 and Ce20Pr80, being consistent with the formation of oxychlorides. The increases in the $Pr^{3+}$ percentages were also in agreement with the formation of PrOCl. On the contrary, the Cl/(Ce + Pr) atomic ratios of the remaining catalysts were far below 1, in agreement with the lower chlorination suffered by Ce100, Ce80Pr20 and Ce50Pr50 oxides. As observed in Fig. 10, the Ce100 and Ce80Pr20 catalysts presented an additional chlorine peak at 206.1 eV that could be tentatively assigned to chlorate species ($Ce(ClO_3)_n$) [32]. This value of binding energy is in close agreement with that reported in the literature for other chlorates (ca for $KClO_3$, 206.5 eV) [33].

In Fig. 11, the Cl/(Ce + Pr) atomic ratio was plotted against the Pr content of samples, and the degree of surface chlorination matched quite well with previous structural characterisation. The Pr-rich formulations presented a higher concentration of chlorine on the surface, and also suffered important structural changes as deduced by bulk techniques, while Ce-rich compositions accumulated a lower amount of chlorine on the surface. The lowest chlorine concentration on surface, after three DCE oxidation cycles between 150 and 500 °C, corresponded to the Ce50Pr50 catalyst, which was also the most active and stable formulation. The surface

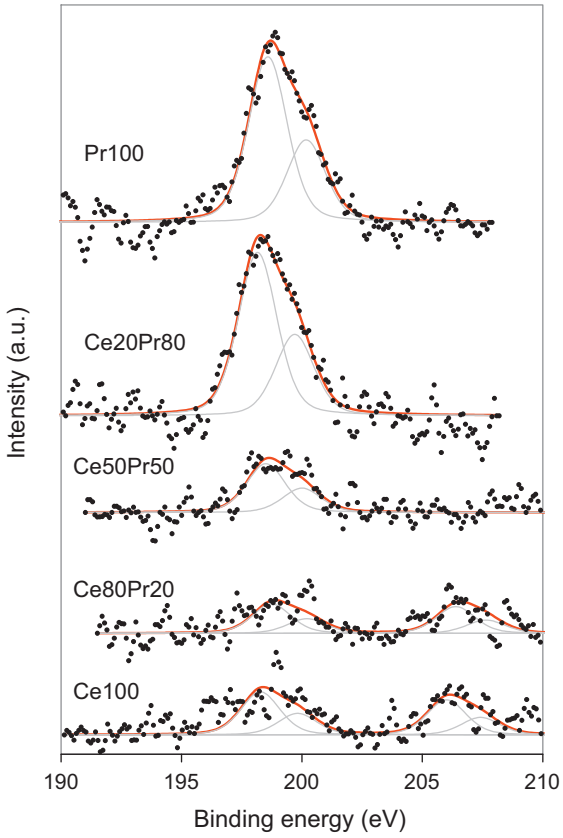


**Fig. 10.** XPS spectra ($Cl_{2p}$ core level) of used catalysts, after three DCE oxidation cycles between 150 and 500 °C.

concentration of chlorine on this sample remained low even after the 115 h lifetime test at 335 °C.

The accumulation of chlorine on the surface during the course of the DCE combustions occurred at expenses of oxygen, as deduced from the decrease in the O/(Ce + Pr) ratios for all samples (see Table 4). A more detailed analysis of the surface oxygen was obtained from Fig. 12, where the $O_{1s}$ energy range was depicted for both fresh and used catalysts. As a general trend, the intensity of the $O_{1s}$ signals was much lower after the DCE combustions than that in the fresh catalysts, in agreement with the surface oxygen depletion (note that the *Y*-axis length is 3 times larger in Fig. 12a (before reaction) than in Fig. 12b (after reactions)). All $O_{1s}$ profiles showed two peaks, which were attributed to lattice oxygen (low energy peak) and to "loosely-bound" oxygen (carbonates,

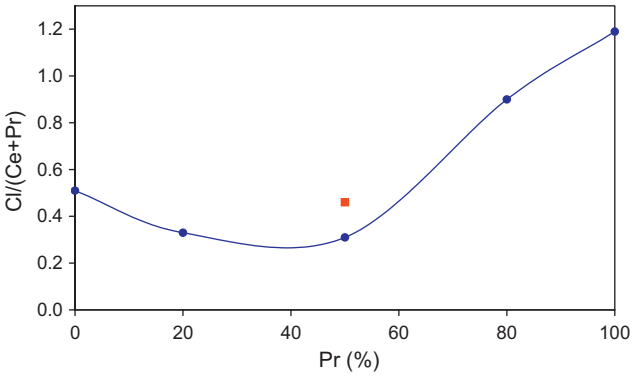


**Fig. 11.** XPS analysis of the surface chlorine concentration as a function of the Pr molar percentage (with regard to Ce + Pr). (Circles: after three DCE oxidation cycles between 150 and 500 °C; squares: after a 115 h lifetime test at 335 °C.)

**Table 4**
Results of the XPS surface characterisation of fresh and used catalysts, after three DCE oxidation cycles between 150 and 500 °C (values calculated from atomic concentrations).

| Catalyst | Ce/Pr* | Cl (%) | Cl/(Ce + Pr) | O/(Ce + Pr) | $Ce^{3+}$ (%) | $Pr^{3+}$ (%) |
|---|---|---|---|---|---|---|
| Ce100 (fresh) | – | – | – | 2.62 | 41.1 | – |
| Ce100 (used) | – | 10.8 | 0.51 | 2.31 | 35.8 | – |
| Ce80Pr20 (fresh) | 1.84 (4) | – | – | 2.18 | 30.6 | 47.9 |
| Ce80Pr20 (used) | 1.97 (4) | 11.6 | 0.33 | 0.85 | 34.0 | 67.5 |
| Ce50Pr50 (fresh) | 0.66 (1) | – | – | 2.58 | 31.6 | 26.4 |
| Ce50Pr50 (used) | 0.70 (1) | 8.6 | 0.27 | 1.12 | 32.7 | 93.4 |
| Ce20Pr80 (fresh) | 0.22 (0.25) | – | – | 2.56 | 32.4 | 8.0 |
| Ce20Pr80 (used) | 0.44 (0.25) | 18.8 | 0.85 | 1.11 | 45.6 | 55.1 |
| Pr100 (fresh) | – | – | – | 2.51 | – | 35.3 |
| Pr100 (used) | – | 24.8 | 1.19 | 1.09 | – | 94.9 |

* Nominal ratios in parenthesis.

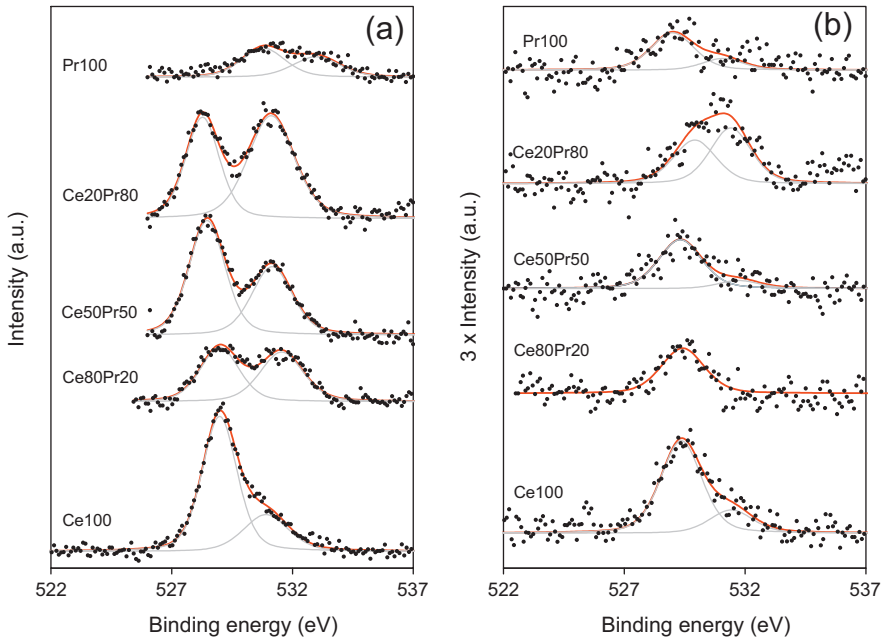


**Fig. 12.** XPS spectra ($O_{1s}$ core level) of fresh (a) and used catalysts (after three DCE oxidation cycles between 150 and 500 °C) (b).

hydroxyls, adsorbed oxygen, peroxide and superoxide groups...), respectively. The loosely-bond oxygen peak decreased significantly or even disappeared after the DCE combustion tests.

## 4. Conclusions

In summary, the results presented in this paper show that Ce/Pr mixed oxides can be considered promising catalysts for DCE (1000 ppm) oxidation at relatively high space velocity (30,000 $h^{-1}$). The activity trend of examined oxides ($Ce_{0.8}Pr_{0.2}O_2$, $Ce_{0.5}Pr_{0.5}O_2$, $Ce_{0.2}Pr_{0.8}O_2$, $CeO_2$ and $PrO_{2-x}$) varied with the number of reaction cycles between 150 and 500 °C. While fresh $PrO_{2-x}$, $Ce_{0.2}Pr_{0.8}O_2$ and $Ce_{0.5}Pr_{0.5}O_2$ samples were highly active, only the $Ce_{0.5}Pr_{0.5}O_2$ mixed oxide showed a markedly stable behaviour after three consecutive cycles. The decrease in activity of Pr-rich oxides was assigned to severe chlorination with PrOCl formation. Interestingly, the $Ce_{0.5}Pr_{0.5}O_2$ sample exhibited a good performance at 335 °C during 115 h time on stream with no apparent deactivation. After reaction only minor structural changes were found with a limited chlorination, which essentially affected the surface of the oxide.

## Acknowledgements

The authors thank the financial support of Generalitat Valenciana (Project Prometeo 2009/047), UPV/EHU-Gobierno Vasco (Project SAIOTEK S-PE11UN025), and EU (FEDER funding). N.G.H. wishes to thank Generalitat Valenciana her Ph.D. grant within VAL i+d Program.

## References

[1] Thematic Strategy on Air Pollution, Communication from the Commission to the Council and The European Parliament, Commission of the European Communities, COM (2005) 446 final, Brussels, 2005.
[2] P. Hunter, S.T. Oyama, Control of Volatile Organic Compound Emissions, John Wiley, New York, 2000.
[3] J.J. Spivey, in: G. Ertl (Ed.), Handbook of Heterogeneous Catalysis, vol. 5, Wiley-VCH Verlag, Weinheim, 2008, pp. 2394–2411.
[4] J.I. Gutiérrez-Ortiz, B. de Rivas, R. López-Fonseca, J.R. González-Velasco, Applied Catalysis B 65 (2006) 191–200.
[5] Q. Dai, X. Wang, G. Lu, Catalysis Communications 8 (2007) 1645–1649.
[6] Q. Huang, X. Xue, R. Zhou, Journal of Hazardous Materials 183 (2010) 694–700.
[7] J. Mikulova, S. Rossignol, J. Barbier, D. Duprez, C. Kappenstein, Catalysis Today 124 (2007) 185–190.
[8] K.M. Ryan, J.P. McGrath, R.A. Farrell, W.M. O'Neill, C.J. Barnes, M.A. Morris, Journal of Physics: Condensed Matter 15 (2003) L49–L58.
[9] Q. Wang, B. Zhao, L. Guangfeng, R. Zhou, Environmental Science and Technology 44 (2010) 3870–3875.
[10] Z. Song, W. Liu, H. Nishiguchi, A. Takami, K. Nagaoka, Y. Takita, Applied Catalysis A 329 (2007) 86–92.
[11] E. Rohart, V. Belliere-Baca, K. Yokota, V. Harle, C. Pitois, Topics in Catalysis 42–43 (2007) 71–75.
[12] V. Rico-Perez, S. Parres-Esclápez, M.J. Illán-Gómez, C. Salinas-Martínez de Lecea, A. Bueno-López, Applied Catalysis B 107 (2011) 18–25.
[13] M.-F. Luo, Z.-L. Yan, L.-Y. Jin, Journal of Molecular Catalysis A 260 (2006) 157–162.

[14] B.M. Reddy, G. Thrimurthulu, L. Katta, Y. Yamada, S.-E. Park, Journal of Physical Chemistry C 113 (2009) 15882–15890.
[15] H. Li, G. Lu, Y. Wang, Y. Guo, Y. Guo, Catalysis Communications 11 (2010) 946–950.
[16] K. Krishna, A. Bueno-López, M. Makkee, J.A. Moulijn, Applied Catalysis B 75 (2007) 210–220.
[17] G. Zhang, Z. Zhen, J. Xu, J. Zheng, J. Liu, G. Jiang, A. Duan, H. He, Applied Catalysis B 107 (2011) 302–315.
[18] K.S. Go, Y. Kim, S.R. Son, S.D. Kim, Chemical Engineering Science 65 (2010) 499–503.
[19] WHO Regional Office for Europe, Air Quality Guidelines, Chapter 5.6, second ed., WHO Regional Publications, European Series, No. 91, Copenhagen, 2000.
[20] P.H. Taylor, B. Dellinger, C.C. Lee, Environmental Science and Technology 24 (1990) 316–328.
[21] R. López-Fonseca, J.I. Gutiérrez-Ortiz, M.A. Gutiérrez-Ortiz, J.R. González-Velasco, Journal of Chemical Technology and Biotechnology 78 (2003) 15–22.
[22] B. de Rivas, R. López-Fonseca, C. Jiménez-González, J.I. Gutiérrez-Ortiz, Journal of Catalysis 281 (2011) 88–97.
[23] M. Romeo, K. Bak, J. El Fallah, F. le Normand, L. Hilaire, Surface and Interface Analysis 20 (1993) 508–512.
[24] H. Borchet, Y.V. Frolova, V.V. Kaichev, I.P. Prosvirin, G.M. Alikina, A.I. Lukashevich, V.I. Zaikovskii, E.M. Moroz, S.N. Trukhan, V.P. Ivanov, E.A. Paukshtis, V.I. Bukhtiyarov, V.A. Sadykov, Journal of Physical Chemistry B 109 (2005) 5728–5738.
[25] B. de Rivas, R. López-Fonseca, M.A. Gutiérrez-Ortiz, J.I. Gutiérrez-Ortiz, Applied Catalysis B 104 (2011) 373–381.
[26] H.C. Yang, H.C. Eun, Y.Z. Cho, H.S. Lee, I.T. Kim, Thermochimica Acta 484 (2009) 77–81.
[27] Q. Dai, X. Wang, G. Lu, Applied Catalysis B 81 (2008) 192–202.
[28] T. Aitasalo, J. Hölsä, M. Lastusaari, J. Legendziewicz, L. Lehto, J. Lindén, M. Marysko, Journal of Alloys and Compounds 380 (2004) 296–302.
[29] J. Hölsä, E. Kestilä, K. Koshi, H. Rahiala, Journal of Alloys and Compounds 225 (1995) 193–197.
[30] J. Hölsä, K. Koshi, S. Makkonen, E. Säilynoja, H. Rahiala, Journal of Alloys and Compounds 249 (1997) 217–220.
[31] M.P. Yeste, Sigüenza, Ph.D. Thesis, University of Cádiz, Spain, 2009.
[32] http://www.lasurface.com/database/elementxps.php?bib=111, accessed on January 20 2012.
[33] C.D. Wagner, J.F. Moulder, L.E. Davis, W.M. Riggs, Handbook of X-ray Photoelectron Spectroscopy, Perking-Elmer Corporation, Physical Electronics Division, 1978.